

SEISMIC VELOCITY/POLARIZATION ESTIMATION AND POLARIZED WAVEFIELD SEPARATION

D. Donno^(1,2), *A. Nehorai*⁽²⁾ and *U. Spagnolini*⁽¹⁾

⁽¹⁾Dipartimento di Elettronica e Informazione, Politecnico di Milano, Milano (Italy)

⁽²⁾ECE Department, University of Illinois at Chicago, Chicago (IL, USA)

ABSTRACT

This paper addresses the problem of estimating the shape parameters of seismic wavefields in linear array for the separation of waves by exploiting the diversity of the polarization state and propagation velocity between wavefields. We propose a method based on the shift-invariance properties of multiple wavefields impinging on a uniform linear array of sensors to separate different waves, by jointly estimating the velocity and polarization parameters. Furthermore, the surface waves are removed using a spatial filter specifically designed to exploit velocity and polarization of different waves. We introduce a model for wideband polarized signals received by an array of three-components sensors used as a framework for implementing the proposed algorithms. Examples on simulated and experimental data illustrate the applicability of the proposed methods.

1. INTRODUCTION

Geophysical exploration maps the characteristics of the subsurface layers from the seismic wavefields registered by surface sensors. However, only the waves reflected by the subsurface layers contain interesting information about the subsurface. Estimating and separating spurious surface waves (technically referred as *ground-roll*) from a seismic recording makes reflected volume waves significantly easier to be recognized and used for imaging.

Compared with volume waves, surface waves are characterized by a lower velocity and a higher polarization (they are elliptically polarized with ellipticity $\varepsilon > 0.5$). Therefore, surface waves filtering should exploit all these characteristics to be effective. Conventional methods for surface waves suppression take into account velocity (e.g., by f-k filters [1]) or polarization [2] only. A first attempt to employ the joint information on velocity and polarization to separate different seismic wavefields is in [3]. However, for electromagnetic wavefields, several narrowband direction-finding and polarization estimation algorithms have been investigated (see [4], [5] and [6]).

We describe a parametric model for multiple wideband polarized signals received by an array of three-component sensors (Sect. 2) that will be the framework for the proposed methods. We propose (Sect. 3) an algorithm that exploits the shift-invariance properties of the data for the joint estimation of velocity and polarization. Moreover, we define a constrained optimization problem for filtering surface waves from seismic recordings by exploiting the velocity/polarization estimates (Sect. 4). Simulated and experimental data examples show that the velocity/polarization estimation is effective for surface waves separation when the estimates are exploited to design spatial filtering (Sect. 5).

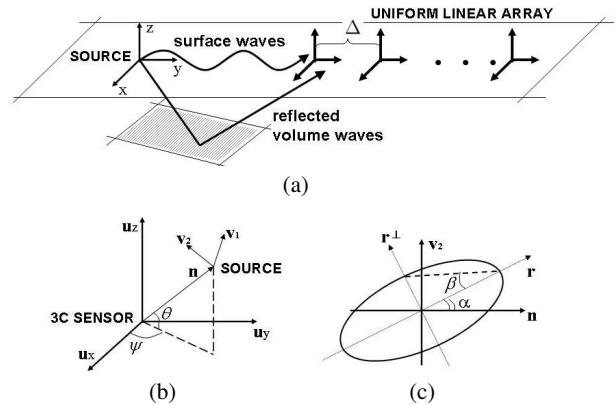


Fig. 1. (a) Geometry of the scenario for the multiple-wavefields multiple-sensors case. (b) The azimuth ψ and elevation θ relate the reference coordinate systems of the sensor $\{u_x, u_y, u_z\}$ and the source $\{n, v_1, v_2\}$. (c) The polarization ellipse in the plane of polarization with the orientation angle α and the ellipticity angle β .

2. PARAMETRIC MODEL FOR WIDEBAND POLARIZED SEISMIC WAVES

The model presented herein is based on parameters describing the polarization properties of the waveforms, as proposed in [7]. An experimental motivation for this model can be found in [8]. Experiment is shown in Fig. 1(a) where a linear array of three-component sensors (3C geophones) measures the wideband seismic wavefields. Each of the wideband wavefields can be described as a combination of narrowband components, thus reducing the wideband problem to L narrowband equivalent problems for each of the frequencies f_l (for $l = 1, \dots, L$) of the input signal.

For the single-wavefield single-sensor model (Fig. 1(b)), let $\mathbf{y}(t) = [y_x(t), y_y(t), y_z(t)]^T$ be the noise-free particle displacement signal at the three-component sensor in one observation period T . By computing the DFT of the signal $\mathbf{y}(t)$, the l -th frequency sample of the output signal in additive Gaussian noise is [7]

$$\mathbf{y}(f_l) = X(f_l)\mathbf{p}(\Phi) + \mathbf{e}(f_l) \quad l = 1, \dots, L \quad (1)$$

where $X(f_l)$ is the source signal in the frequency domain and $\mathbf{p}(\Phi) \in \mathbb{C}^{3 \times 1}$ is the response vector of the sensor (or *polarization vector*) that contains all the information about the polarization state of the wavefields. Polarization depends on the set of angle parameters $\Phi = [\psi, \theta, \alpha, \beta, \gamma]^T$ where, from Fig. 1(b), ψ and θ are the azimuth and elevation angles of the geometry of acquisition, α is the rotation angle of the polarization ellipse (see Fig. 1(c)), β is the ellipticity

angle (the ellipticity is $\varepsilon = \tan \beta \in [-1, 1]$) and γ is the rotation angle of the plane of polarization that enables to describe both longitudinal and transversal polarized waves. The noise is Gaussian: $\mathbf{e}(f_i) \sim CN(0, \sigma^2 \mathbf{I}_3)$.

In the case of d wavefields impinging on a uniform linear array (ULA) of M three-component sensors spaced apart by Δ (see Fig. 1(a)), the l -th frequency sample of the output signal is

$$\mathbf{Y}(f_i) = \mathbf{A}(f_i) \mathbf{X}(f_i) \mathbf{P}(\Theta) + \mathbf{E}(f_i) \quad (2)$$

where $\mathbf{A}(f_i) = [\mathbf{a}(f_i, v_1), \dots, \mathbf{a}(f_i, v_d)]$ and the k -th steering vector is $\mathbf{a}(f_i, v_k) = [1, e^{-j\eta_k f_i}, \dots, e^{-j\eta_k (M-1) f_i}]^T$ with $\eta_k = 2\pi\Delta/v_k$ and v_k is the velocity of the k -th wavefield (for $k = 1, \dots, d$). Matrix $\mathbf{X}(f_i) = \text{diag}[X_1(f_i), \dots, X_d(f_i)]$ accounts for the amplitudes, $\mathbf{P}(\Theta) = [\mathbf{p}(\Phi_1), \dots, \mathbf{p}(\Phi_d)]^T$ is the polarization matrix and $\mathbf{E}(f_i)$ is the noise matrix. From (2), the unknown shape parameters of the k -th wavefield are the velocity v_k and the set of angle parameters $\Phi_k = [\psi_k, \theta_k, \alpha_k, \beta_k, \gamma_k]^T$ that characterizes the polarization vector $\mathbf{p}(\Phi_k)$ of each wavefield.

Stacking the columns of the $M \times 3$ data matrix $\mathbf{Y}(f_i)$ into the $3M \times 1$ vector $\mathbf{z}(f_i)$, we obtain

$$\mathbf{z}(f_i) = \text{vec}(\mathbf{Y}(f_i)) = \mathbf{H}(f_i) \mathbf{x}(f_i) + \mathbf{n}(f_i) \quad (3)$$

where $\mathbf{x}(f_i) = \text{vec}(\mathbf{X}(f_i))$, $\mathbf{n}(f_i) = \text{vec}(\mathbf{E}(f_i))$ and $\mathbf{H}(f_i) = (\mathbf{P}(\Theta)^T \otimes \mathbf{A}(f_i))$ describes the array manifold that depends on the polarization and the velocity of each of the d wavefields (symbol \otimes denotes the Kronecker matrix product).

3. JOINT ESTIMATION OF VELOCITY AND POLARIZATION

Here, we propose a shift-invariance based method for the joint velocity and polarization estimation. Differently from ESPRIT [9] that is limited to processing narrowband data, here we exploit the shift-invariance over all the L frequency samples having the same shape parameters. Within this section, dependency on frequency is omitted only for sake of notation simplicity.

Let the singular value decomposition of the data matrix \mathbf{Y} in (2) be $\mathbf{Y} = \mathbf{U} \Sigma \mathbf{V}^H$, where \mathbf{U} and \mathbf{V} are the unitary matrices formed respectively with the left and right singular vectors of \mathbf{Y} , while Σ is a $M \times 3$ diagonal matrix that contains the singular values of \mathbf{Y} , sorted in decreasing order. Since the eigenvectors associated with the d largest eigenvalues of \mathbf{Y} are known to span the signal subspace, matrix \mathbf{Y} can thus be partitioned into signal and noise subspace matrices, resulting in $\mathbf{Y} = \mathbf{U}_S \Sigma_S \mathbf{V}_S^H + \mathbf{U}_N \Sigma_N \mathbf{V}_N^H$.

The signal subspace $\mathbf{U}_S \Sigma_S \mathbf{V}_S^H$ can be identified with the noise-free signal of \mathbf{Y} , hence $\mathbf{U}_S \Sigma_S \mathbf{V}_S^H \simeq \mathbf{A} \mathbf{X} \mathbf{P}$. It follows that the d left singular vectors of \mathbf{Y} can be written as

$$\mathbf{U}_S = \mathbf{A} \mathbf{X} \mathbf{C} \quad (4)$$

where $\mathbf{C} = \mathbf{P} \mathbf{V}_S \Sigma_S^{-1}$. This decomposition preserves the velocity and polarization information into \mathbf{U}_S . Moreover, \mathbf{U}_S has a structure similar to that of \mathbf{Y} , consequently a shift-invariance technique can be applied to \mathbf{U}_S to estimate the shape parameters of the wavefields.

Let $\mathbf{U}_S^{(1)}$ and $\mathbf{U}_S^{(2)}$ be two subsets of the data \mathbf{U}_S . For an array of M elements, $\mathbf{U}_S^{(1)}$ and $\mathbf{U}_S^{(2)}$ are chosen to be one the shifted copy of the other, by taking the first and the last $M-1$ sensors, respectively. In accordance with the shift invariance property between two subsets, the relationship between $\mathbf{U}_S^{(1)}$ and $\mathbf{U}_S^{(2)}$ is linear and

depends on the wavefields velocity and polarization. Similar to the ESPRIT method, the two subsets $\mathbf{U}_S^{(1)}$ and $\mathbf{U}_S^{(2)}$ differ only by a phase shift that can be collected (for all the d wavefields) into the diagonal matrix $\mathbf{D} = \text{diag}[e^{-j\eta_1 f}, \dots, e^{-j\eta_d f}]$. The two subsets can be modelled according to (2) as

$$\mathbf{U}_S^{(1)} = \mathbf{A}^{(1)} \mathbf{X} \mathbf{C} \quad (5)$$

$$\mathbf{U}_S^{(2)} = \mathbf{A}^{(2)} \mathbf{X} \mathbf{C} = \mathbf{A}^{(1)} \mathbf{D} \mathbf{X} \mathbf{C} = \mathbf{A}^{(1)} \mathbf{X} \mathbf{D} \mathbf{C} \quad (6)$$

where $\mathbf{A}^{(1)}$ and $\mathbf{A}^{(2)}$ are the $(M-1) \times d$ subsets of the array response \mathbf{A} . The relationship between $\mathbf{U}_S^{(1)}$ and $\mathbf{U}_S^{(2)}$ can be reduced to $\mathbf{U}_S^{(1)} \mathbf{T} = \mathbf{U}_S^{(2)}$, where the $d \times d$ shifting matrix \mathbf{T} has to be estimated by least squares (LS) or total least-squares (TLS) method. Rearranging the subsets (5) and (6) and considering full-rank matrices, it yields

$$\mathbf{T} = \mathbf{C}^{-1} \mathbf{D} \mathbf{C}, \quad (7)$$

thus matrix \mathbf{T} contains the information of polarization and velocity for each of the wavefields. In particular, eigenvalues of \mathbf{T} are unit-amplitude complex values whose phases depend on the velocities v_k , while the eigenvectors of \mathbf{T} in \mathbf{C}^{-1} are related to the polarization of the wavefields by $\mathbf{P} = \mathbf{C} \Sigma_S \mathbf{V}_S^H$. As a result, for each frequency sample, velocity and polarization are estimated and automatically paired. In Section 5, when discussing numerical results we will show that once estimated the shape parameters, the surface waves can be easily separated from volume waves in the velocity/ellipticity plane.

To increase the number of wavefields that can be estimated and to obtain a more accurate estimate of the signal subspace, it is common practice to use spatial smoothing techniques (see for instance [9]).

4. VELOCITY/POLARIZATION CONSTRAINED BROADBAND BEAMFORMING

The problem of spatial filtering is to find the matrix of weights \mathbf{w} such that the desired signal \mathbf{x} is estimated from a linear combination of the $3ML \times 1$ observed data vector $\mathbf{z} = [\mathbf{z}(f_1)^T, \dots, \mathbf{z}(f_L)^T]^T$

$$\hat{\mathbf{x}} = \mathbf{w}^H \mathbf{z}, \quad (8)$$

where $\mathbf{w} = [\mathbf{w}_1^T, \dots, \mathbf{w}_L^T]^T$. Filtering of the interfering wavefields is achieved by linearly constrained minimum variance (LCMV) beamforming:

$$\hat{\mathbf{w}} = \arg \min_{\mathbf{w}} \left\{ \mathbf{w}^H \mathbf{R}_z \mathbf{w} \right\} \quad \text{subject to } \mathbf{K}^H \mathbf{w} = \mathbf{F} \quad (9)$$

where $\mathbf{R}_z = E \{ \mathbf{z} \mathbf{z}^H \}$, matrix \mathbf{K} accounts for the constraints and \mathbf{F} for the desired response, resulting in

$$\hat{\mathbf{w}}^H = \mathbf{F}^H (\mathbf{K}^H \mathbf{R}_z \mathbf{K})^\dagger \mathbf{K}^H \mathbf{R}_z^\dagger \quad (10)$$

where the symbol \dagger indicates the pseudo-inverse of the corresponding matrix.

The solution (10) is valid for wideband signals. However, choosing the constraint matrix \mathbf{K} in (9) to be block diagonal $\mathbf{K} = \text{diag}[\mathbf{K}_1, \dots, \mathbf{K}_l, \dots, \mathbf{K}_L]$, then the weights $\{\mathbf{w}_l\}_{l=1}^L$ are constrained independently and the wideband constraint $\mathbf{K}^H \mathbf{w} = \mathbf{F}$ can be reduced to a set of L constraints $\mathbf{K}_l^H \mathbf{w}_l = \mathbf{F}_l$, one for each of the L frequency samples of the signal. Therefore, the broadband beamformer can be viewed as L narrowband beamforming that produces the frequency domain filtered data $\hat{\mathbf{x}}(f_l) = \mathbf{w}_l^H \mathbf{z}(f_l)$ for $l = 1, \dots, L$. The solution for the l -th narrowband problem is similar to (10):

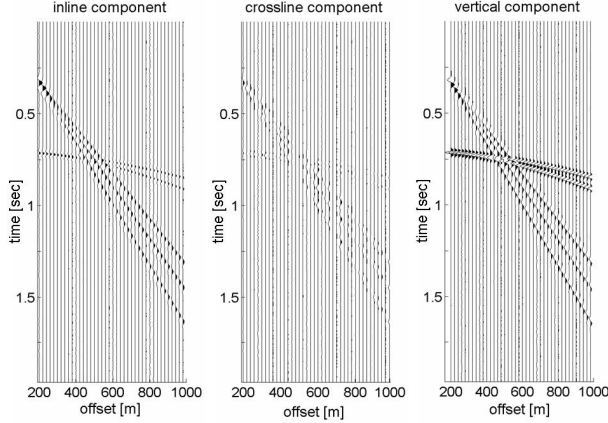


Fig. 2. Original simulated data with mis-positioning: in-line $y_x(t)$ (left), cross-line $y_y(t)$ (center) and vertical $y_z(t)$ (right) components.

$\hat{\mathbf{w}}_l^H = \mathbf{F}_l^H (\mathbf{K}_l^H \mathbf{R}_{z_l}^\dagger \mathbf{K}_l)^\dagger \mathbf{K}_l^H \mathbf{R}_{z_l}^\dagger$. The choices of the matrices \mathbf{F}_l and \mathbf{K}_l for the l -th narrowband beamformer to satisfy the constraint in (9) are specified below.

Velocity/polarization constraints: Let the estimated polarization matrix $\hat{\mathbf{P}}$ be partitioned as $\hat{\mathbf{P}} = \begin{bmatrix} \hat{\mathbf{P}}_{sur} \\ \hat{\mathbf{P}}_{vol} \end{bmatrix}$, where $\hat{\mathbf{P}}_{sur}$ and $\hat{\mathbf{P}}_{vol}$ are the polarization matrices for surface and volume waves, respectively. The same partition for the estimated steering matrix $\hat{\mathbf{A}}$ results in $\hat{\mathbf{A}} = \begin{bmatrix} \hat{\mathbf{A}}_{sur} & \hat{\mathbf{A}}_{vol} \end{bmatrix}$. Notice that the dimensions of the partition matrices are chosen by employing clustering techniques [10], as it will be shown in Section 5.

The beamformer response is constrained to have unitary gain for the pairs velocity/polarization relative to volume waves, and zero gain for the estimates of surface waves. If we had only one wavefield, the constraints would be

$$\left(\hat{\mathbf{p}}_{vol}^T \otimes \hat{\mathbf{a}}_{vol} \right)^H \mathbf{w}_l = 1 \quad \text{and} \quad \left(\hat{\mathbf{p}}_{sur}^T \otimes \hat{\mathbf{a}}_{sur} \right)^H \mathbf{w}_l = 0 \quad (11)$$

where $\hat{\mathbf{p}}_{vol}$ and $\hat{\mathbf{p}}_{sur}$ are the 3×1 estimated polarization vectors defined as in (1), while $\hat{\mathbf{a}}_{vol}$ and $\hat{\mathbf{a}}_{sur}$ are the $M \times 1$ estimated steering vectors.

With more than one wavefield, the constraints in (11) can be written into a matrix form as

$$\left(\begin{bmatrix} \hat{\mathbf{P}}_{sur} \\ \hat{\mathbf{P}}_{vol} \end{bmatrix}^T \otimes \begin{bmatrix} \hat{\mathbf{A}}_{sur} & \hat{\mathbf{A}}_{vol} \end{bmatrix} \right)^H \mathbf{w}_l = \mathbf{F}_l. \quad (12)$$

Smooth constraints: The velocity/polarization constraints alone are inadequate to ensure good performance in presence of errors in the estimation of the shape parameters as well as in the calibration of the sensors. We propose to add *derivative* constraints [11] by forcing the derivative of the array manifold $\mathbf{H}(f_l) = (\mathbf{P}^T \otimes \mathbf{A}(f_l))$ with respect to velocity v and polarization angle β to be zero in order to achieve a maximally flat response of the filter over a region around the peaks of the lobes. Therefore, the matrix of constraints $\mathbf{K}_{l,der}$ has the form

$$\mathbf{K}_{l,der} = \left[\mathbf{P}^T \otimes \mathbf{A}, \frac{d}{dv} (\mathbf{P}^T \otimes \mathbf{A}), \frac{d}{d\beta} (\mathbf{P}^T \otimes \mathbf{A}) \right] \quad (13)$$

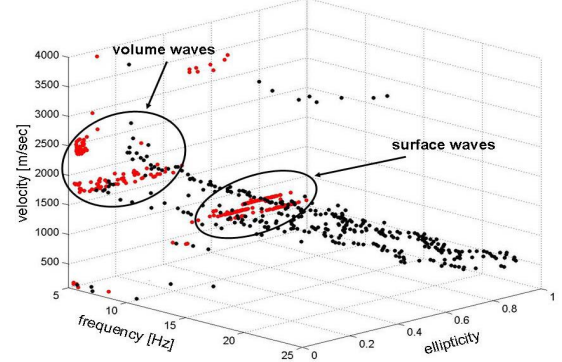


Fig. 3. Wavefield separation ($d = 5$) in the velocity vs. ellipticity plane $\{\hat{v}_k, \hat{\epsilon}_k\}$ for several frequency samples. Red points are the projection of the frequency-dependent estimates (in black) onto the velocity-ellipticity plane.

and the desired matrix response $\mathbf{F}_{l,der}$ imposes zeros in correspondence of the derivatives of the array manifold $\mathbf{H}(f_l)$

$$\mathbf{F}_{l,der} = \begin{bmatrix} \mathbf{F}_l \\ \mathbf{0} \\ \mathbf{0} \end{bmatrix} \quad (14)$$

5. EXPERIMENTAL RESULTS

Examples on simulated and field data show the applicability of the proposed methods to estimate the shape parameters of seismic waves and to separate polarized wavefields.

The three components of the original synthetic data are shown in Fig. 2. The experiment consists of an in-line shot which produces two reflected volume waves and three surface waves. The Ricker waveform has been modelled using different frequencies [1] for surface waves ($f_c = 20\text{Hz}$) and volume waves ($f_c = 30\text{Hz}$). Sampling period is 5msec. The sensor array is made of $M = 40$ 3C geophones spaced apart by $\Delta = 20\text{m}$. A zero mean uncorrelated Gaussian noise with noise power σ^2 is added, with signal to noise ratio $SNR = \frac{E}{\sigma^2} = 10\text{dB}$, where E is the energy of the waveform for surface and volume waves. Moreover, we suppose to have array perturbations, with each sensor being affected by an angular rotation of the horizontal sensor components, distributed as a zero-mean Gaussian density with standard deviation of 20deg with respect to its nominal position.

Fig. 3 shows the velocity vs. ellipticity estimates, obtained using the shift invariance method, versus the frequency. The projections of these estimates onto the velocity/ellipticity plane (the red points in Fig. 3) show that a simple method based on a velocity/polarization threshold is sufficient to separate surface waves from the volume waves. Moreover, clustering techniques [10] can be used to create a partition of the estimates and find the dimensions of the two subgroups.

The results after applying beamforming to the data of Fig. 2 are in Fig. 4. The three surface wavefields have been totally removed. However, in the result after the application of the *velocity/polarization* constrained beamformer (on the left) only one of the two volume waves is present. This happens because in an environment with mis-positioning of the sensors, the estimation of the shape parameters suffers from higher uncertainty, thus affecting the construction of the filter whose main beam position does not coincide

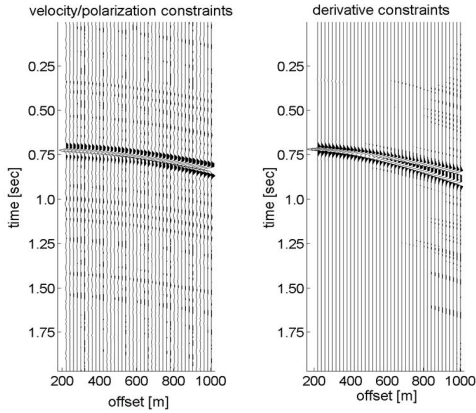


Fig. 4. Vertical component $y_z(t)$ of the simulated data: after application of *velocity/polarization* constrained beamformer (left) and after application of *derivative* constrained beamformer (right).

with the actual position of the wavefield to be preserved. The result after applying the *derivative* constrained beamformer (on the right of Fig. 4) gives a better performance as the beam pattern in correspondence of peaks and nulls is smoother, thus allowing for errors.

The field collected seismic data on the left of Fig. 5(b) is a land measurement from an in-line survey. The array of sensors is composed of $M = 320$ three-component sensors spaced apart by $\Delta = 30\text{m}$. The source point is located between the 160-th and the 161-st sensor, the sampling period is 4msec. The data is corrupted by strong surface waves with velocities from 238m/sec to 834m/sec. Other linear events with higher velocity (around 2100m/sec) are visible, and we can also notice the reflected events we are interested in enhancing.

In Fig. 5(a) velocity is plotted versus ellipticity for each frequency, in the range from 5Hz to 25Hz. Notice that surface wave estimates can be reliably separated from the volume waves ones, even if these estimates are clearly more scattered when compared with the simulated data. Moreover, each estimate can be classified into a group employing clustering algorithms. The result after application of the derivative constrained beamformer (on the right of Fig. 5(b)) that the surface waves have been totally removed from the central section of the recording and that the volume waves have been enhanced. However, some visible artifacts are still due to a poor estimation of the parameters of interest and to a consequent beamforming filter inadequate to fully remove the interference.

6. CONCLUSIONS

In this paper, we proposed a parametric model for the multi-component wideband polarized signal. We developed a method which exploits the shift-invariance of linear arrays to estimate and automatically pair the velocity and polarization parameters of polarized wavefields. Moreover, we showed the efficiency of the method to separate mixed seismic wavefields into their constituent wave modes. We proposed a velocity/polarization constrained broadband beamformer to suppress the interference from surface waves and we introduce additional smoothing constraints to allow for reliable filtering when estimates are affected by uncertainty. Techniques for the calibration of the array of sensors is one of the open issues related to practical application that needs to be further investigated to reduce errors in the parameters estimation and in the beamforming.

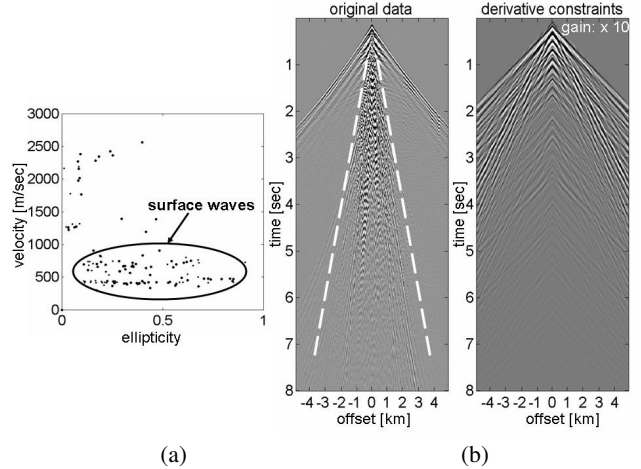


Fig. 5. Experimental seismic measurements: (a) Wavefield separation in the velocity vs. ellipticity plane. (b) Vertical component of the experimental data before (left) and after (right) *derivative* constrained beamformer (surface waves are within dashed lines section).

7. REFERENCES

- [1] O. Yilmaz, *Seismic Data Analysis*, SEG, 2001.
- [2] M. Becquey and M. Manin, "Ellipticity filter for ground-roll removal," in *58th Mtg. Eur. Assn. Geosci. Eng.*, Amsterdam, Jun. 1996.
- [3] J. Picheral, *High resolution methods for joint angle and delay estimation*, Ph.D. thesis, Université de Paris XI - SUPELEC, 2003.
- [4] A. Nehorai and E. Paldi, "Vector-sensor array processing for electromagnetic source localization," *IEEE Trans. Signal Processing*, vol. 42, pp. 376–398, Feb. 1994.
- [5] J. Li and R. T. Compton, "Angle and polarization estimation using ESPRIT with a polarization sensitive array," *IEEE Trans. Antennas Propagat.*, vol. 39, pp. 1376–1383, Sep. 1991.
- [6] K. T. Wong and M. D. Zoltowski, "Closed-form direction finding and polarization estimation with arbitrarily spaced electromagnetic vector-sensors at unknown locations," *IEEE Trans. Antennas Propagat.*, vol. 48, pp. 671–681, May 2000.
- [7] S. Anderson and A. Nehorai, "Analysis of a polarized seismic wave model," *IEEE Trans. Signal Processing*, vol. 44, pp. 379–386, Feb. 1996.
- [8] T. H. Kebo, M. N. Toksos, C. H. Cheng, and R. M. Turpening, "Wave dynamics in a Gulf coast VSP," in *Handbook of Geophysical Exploration*, vol. 14B, pp. 205–235. Geophysical Press, 1984.
- [9] R. Roy and T. Kailath, "ESPRIT - Estimation of signal parameter via rotational invariance techniques," *IEEE Trans. Acoust., Speech, Signal Processing*, vol. 37, pp. 984–995, Jul. 1989.
- [10] J. A. Hartigan, *Clustering Algorithms*, John Wiley & Sons, New York, 1975.
- [11] M. H. Er and A. Cantoni, "Derivative constraints for broadband element space antenna array processors," *IEEE Trans. Acoust., Speech, Signal Processing*, vol. 31, pp. 1378–1393, Dec. 1983.